

# Magnon spectrum of altermagnets: Time-dependent matrix product states vs. linearized Holstein-Primakoff calculations unravelling spontaneous magnon decay

Federico Garcia-Gaitan, Ali Kefayati, John Q. Xiao, and Branislav K. Nikolić\*  
*Department of Physics and Astronomy, University of Delaware, Newark, DE 19716, USA*

The energy-momentum dispersion of magnons, viewed as noninteracting and, therefore, infinitely long-lived quasiparticles describing collective low-energy excitations of magnetic materials, is often presented as sharp bands obtained from the effective quantum spin Hamiltonian, after being simplified via linearized Holstein-Primakoff (HP) transformations. However, magnons are prone to many-body interactions with other quasiparticles—such as electrons, phonons or other magnons—which can lead to their spontaneous decay, i.e., renormalization of sharp bands and their broadening as the signature of finite quasiparticle lifetime. The magnon-magnon interactions are particularly important in antiferromagnets, and they could also affect newly classified altermagnets sharing many features with collinear antiferromagnets. On the other hand, sharp bands of noninteracting chiral magnons in RuO<sub>2</sub>, as the canonical example of altermagnets, have been very recently predicted [L. Šmejkal *at al.*, Phys. Rev. Lett. **131**, 256703 (2023)]. Here, we employ nonperturbative numerically (quasi)exact quantum many-body calculations, via time-dependent matrix product states (TDMPS), to obtain magnon spectral function of RuO<sub>2</sub>. These calculations produce a broadened magnon dispersion, which overlaps with linearized HP theory sharp bands *only* at edges/center of the Brillouin zone. Substantially deviating otherwise, the TDMPS calculations also produce flat-topped bands. Artificially making exchange interaction within two sublattices of RuO<sub>2</sub> closer in value forces these two spectra to overlap, thereby explaining the origin of the *failure* of linearized HP theory. Such features translate into the difference between their respective density of states, which we also compute and which could be tested by Raman scattering experiments. Finally, we employ popular Landau-Lifshitz-Gilbert (LLG) equation-based *classical* atomistic spin dynamics (ASD) simulations to obtain dynamical structure factor and extract magnon spectrum from it at finite temperature. Despite including magnon-magnon interactions via nonlinearity of LLG equation, ASD simulations *cannot* fully match the TDMPS-computed magnon spectrum due to *nonclassical* effects harbored by antiferro- and altermagnets.

*Introduction.*—The energy-momentum dispersion, standardly plotted as sharp bands along high-symmetry paths in the Brillouin zone, is a fundamental property of quasiparticle collective excitations in solids, such as electrons (in the sense of Landau quasielectrons), phonons and magnons [1]. For example, in the electronic case, diagonalization of single-particle Hamiltonians—such as tight-binding [2] or first-principles ones [3] from density functional theory (DFT)—leads to sharp bands of infinitely long-lived quasielectrons [1]. However, in the presence of strong short- or long-ranged Coulomb interactions, which cannot be captured anymore by effective single particle theories [4], one has to resort to many-body calculations where quasielectrons decay and bands broaden with such broadening signifying inverse lifetime of quasielectrons [4, 5]. Furthermore, when quasielectrons lose their identity completely, one obtains a continuum of energies of the so-called Hubbard bands [4, 5]—see, e.g., Fig. 2 in Ref. [4] for an illustration of sharp bands vs. broadened bands due to moderate electron-electron interactions vs. Hubbard bands due to strong interactions, as well as Fig. 1 in Ref. [5] for angle-resolved photoemission spectroscopy measurement of all three cases.

An analogous situation exists in the case of magnons—quasiparticles introduced by Bloch [6] as a wave-like disturbance in the local magnetic ordering of a magnetic ma-

terial. Their quanta [7] of frequency  $\omega$  behave as bosonic quasiparticles carrying energy  $\hbar\omega$ , spin  $\hbar$  and quasimomentum  $\hbar\mathbf{q}$ . The sharp bands,  $\hbar\omega(\mathbf{q})$  vs.  $\mathbf{q}$  exemplified by red lines in Fig. 1, are standardly computed by extracting parameters of effective spin Hamiltonians [8] from DFT [9], which is then fed into Holstein-Primakoff (HP) [10] transformations that map original spin operators to bosonic ones. By linearizing HP transformations [7] one obtains Hamiltonian quadratic in bosonic operators which is exactly diagonalizable. We also note that very recently developed algorithms can obtain sharp magnon bands from first-principles calculations directly, i.e., without constructing an effective spin Hamiltonian, via GW calculations [11]. However, experiments often measure [12–15] magnon damping, which is a problem of great interest to both basic research [16] and applications in magnonics [17, 18]. The origin of magnon damping can be traced to: magnon-magnon interactions, as described by second-quantized Hamiltonians containing products of three or more bosonic operators [7, 16]); magnon-phonon interactions [14], especially relevant for recently discovered two-dimensional magnetic materials [13]; and magnon-electron interactions in magnetic metals [7, 19–23]. For example, the so-called Landau damping of magnons due to hybridization with the continuum of electronic Stoner excitations, where single-electron spin flips while transitioning from an occupied state with a

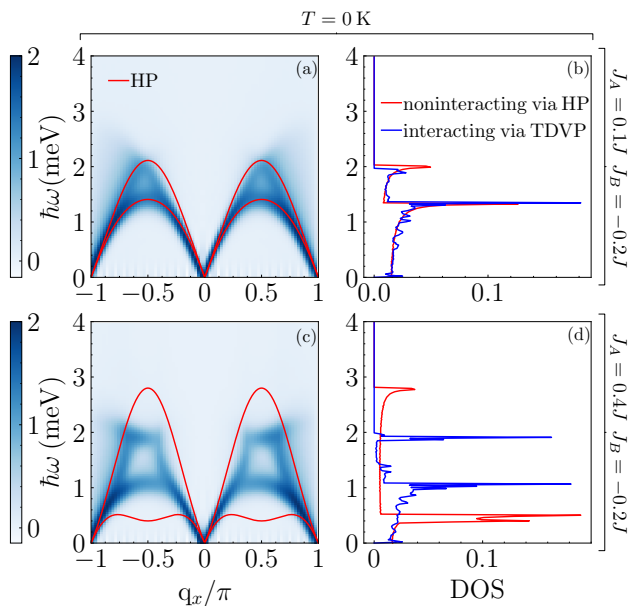


FIG. 1. (a),(c) Magnon energy-momentum dispersion from TDVP-computed spectral function  $A(q_x, \omega)$  [Eq. (2)] of RuO<sub>2</sub> effective spin Hamiltonian [Eq. (3)] defined on quasi-1D ladder of lattice sites (so,  $\mathbf{q} \mapsto q_x$ ). Solid red lines plot conventional [9] sharp magnon dispersion obtained from linearized HP theory for the same lattice. (b),(d) DOS corresponding to magnon dispersion in panels (a),(c), respectively. The difference between the top and bottom row of panels is that in the bottom row we use exchange interactions  $J_A$  and  $J_B$  between quantum spins localized at NN lattice sites obtained from DFT calculations in Ref. [9], while in the top row we artificially make them closer to each other in absolute value. The color bars on the left specify values of TDVP-computed dispersions in panels (a) and (c).

given spin projection to an empty state with an opposite spin projection, has been quantified using either random phase approximation applied to model Hamiltonians [24] or via first-principles methods like time-dependent DFT [19, 20]. Furthermore, the magnon-magnon interactions and thereby induced magnon spontaneous decay [16] are frequently encountered in insulating antiferromagnets [15, 16] and quantum spin liquids [25].

Within quantum many-body theory framework, interaction induced renormalization of magnon energies  $\hbar\omega(\mathbf{q})$  and decay-induced lifetime (i.e., broadening of sharp bands) can be rigorously defined using one-particle retarded Green function (GF) [7, 16]

$$G^{-1}(\mathbf{q}, \omega) = \hbar\omega - \hbar\omega(\mathbf{q}) - \Sigma(\mathbf{q}, \omega), \quad (1)$$

where  $\Sigma(\mathbf{q}, \omega)$  is the self-energy due to interactions. Its real part renormalizes  $\hbar\omega(\mathbf{q})$ , while its imaginary part is responsible for finite lifetime [16]. The self-energy can be computed *perturbatively*, by evaluating selected Feynman diagrams containing loops [16]. Alternatively, one

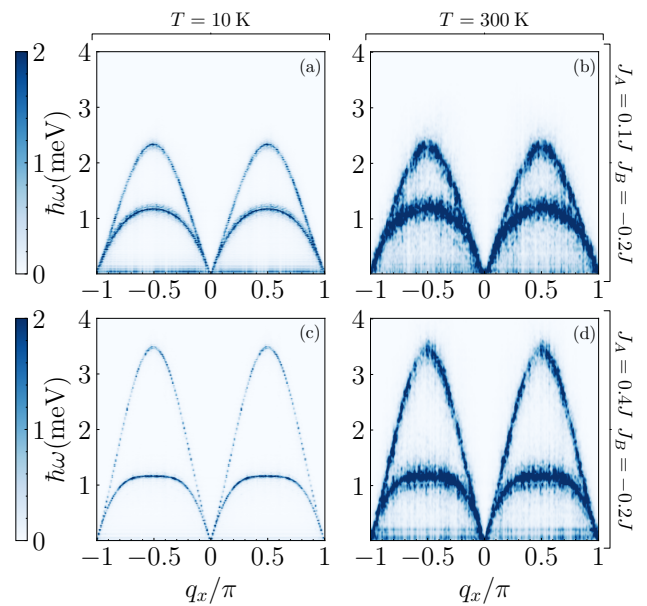


FIG. 2. The same information as in Fig. 1, but obtained from classical ASD [26, 27] calculations of dynamical structure factor [Eq. (9)] at two different temperatures,  $T = 10$  K and  $T = 300$  K. In the stochastic LLG equation [28], underlying ASD simulations [27], we use Gilbert damping  $\alpha = 10^{-4}$ .

can compute the exact GF in Eq. (1) for spin Hamiltonians defined on low-dimensional lattices *nonperturbatively* via numerically (quasi)exact algorithms based on time-dependent matrix product states [29]. These include original time-dependent density matrix renormalization group (tDMRG) [30–33] or time-dependent variational principle (TDVP) [34, 35] (comparison of performance of two methods for different spin Hamiltonians can be found in Ref. [35]). Instead of sharp lines representing bands of noninteracting magnons, one then plots (as we do in Fig. 1 obtained from TDVP) either the spectral function [16]

$$A(\mathbf{q}, \omega) = -\frac{1}{\pi} \text{Im} G(\mathbf{q}, \omega), \quad (2)$$

or the dynamical structure factor  $S(\mathbf{q}, \omega)$ . The latter is directly measurable in neutron scattering experiments [15]. The quantities  $A(\mathbf{q}, \omega)$  and  $S(\mathbf{q}, \omega)$  can also be related to each other [36].

In particular, the very recent analyses [37] have revealed that a widely-used linearized HP theory of noninteracting sharp magnon bands can introduce spurious symmetries, thereby leading to magnon spectrum that is actually quite far away from the correct one obtained from quantum many-body calculations via tDMRG [37]. One reason for this discrepancy is generated when the Heisenberg effective spin Hamiltonian contains further than nearest-neighbor (NN) exchange interactions between localized spins, and they are not equal to each

other. Another situation where linearized HP theory could break down is in antiferromagnets with very different exchange interactions within two sublattices [37]. This is precisely the situation encountered in RuO<sub>2</sub> as a canonical example of altermagnetic materials [38, 39]. These newly established class of magnets was originally considered [40–43] as just another type of collinear antiferromagnets. They have attracted enormous attention due to their unusual fundamental properties and potential applications in spintronics. Akin to ferromagnets, they exhibit time-reversal symmetry breaking and transport properties like the the anomalous Hall effect, tunneling magnetoresistance and magneto-optics [38, 39]. This is due to antiferromagnetic ordering-induced momentum-dependent spin splitting of electronic bands, analogous to materials with spin-orbit-split electronic bands but without requiring noncentrosymmetric crystals and high atomic number elements underlying materials with large spin-orbit coupling [41]. The sharp bands of noninteracting magnons of RuO<sub>2</sub> have also been predicted recently [9], exhibiting chirality akin to ferromagnets, but with linear energy-momentum dispersion akin to antiferromagnets. While Landau damping [19, 20, 24] of magnons in RuO<sub>2</sub> was found [9] to be suppressed by the spin-split electronic structure of altermagnets, there remains possibility of magnon damping due to magnon-magnon interactions that were not explored in Ref. [9].

In this Letter, we compute magnon dispersion of RuO<sub>2</sub> for the same effective spin Hamiltonian used in Ref. [9] via three different methods. For reference, we reproduce chiral magnon bands of Ref. [9] using single quasiparticle quantum-mechanical calculations via linearized HP theory [44]. Such sharp bands are then compared [Fig. 1] to magnon spectrum extracted from  $A(q_x, \omega)$  obtained from nonperturbative quantum many-body calculations via TDVP-implemented algorithm [30] for magnonic retarded GF [Eq. (8)] on quasi one-dimensional (1D) ladder of lattice sites hosting localized quantum spins. Finally, we extract magnon spectrum from classical atomistic spin dynamics (ASD) [28] by calculating [26, 27] the dynamical spin structure factor [Eq. (9)] from stochastic Landau-Lifshitz-Gilbert (LLG) equation-based simulations of the same ladder hosting classical spin vectors. The ASD simulations can take into account both magnon-magnon interactions [45] (as the LLG equation is nonlinear) and finite temperature (via noise terms in the LLG equation [28], but only at the *classical* level. Our principal results for quantum-mechanically treated noninteracting (sharp red lines in Fig. 1) and interacting (broadened blue traces in Fig. 1) magnons are shown in Fig. 1. The clas-

sical treatment of interacting magnons (i.e., spin waves), as described by the LLG equation for antiferromagnetic systems [46, 47], is shown in Fig. 2. Prior to discussing these results, we introduce useful concepts and notation.

*Models and Methods.*—We employ the same effective spin Hamiltonian [8] of the Heisenberg type derived in Ref. [9]

$$\hat{H} = J \sum_{\langle ij \rangle} \hat{\mathbf{S}}_i \cdot \hat{\mathbf{S}}_j + J_A \sum_{\langle\langle ij \rangle\rangle_A} \hat{\mathbf{S}}_i \cdot \hat{\mathbf{S}}_j + J_B \sum_{\langle\langle ij \rangle\rangle_B} \hat{\mathbf{S}}_i \cdot \hat{\mathbf{S}}_j, \quad (3)$$

where  $\hat{\mathbf{S}}_i$  is the operator of  $S = 1/2$  spin localized at site  $i$  of the lattice;  $\langle ij \rangle$  denotes the summation over NN sites within two different sublattices of altermagnet; and  $\langle\langle ij \rangle\rangle_A$  and  $\langle\langle ij \rangle\rangle_B$  denotes the summation over NN sites within a single sublattice. The specific values of exchange interactions  $J_A = 1.25$  meV and  $J_B = -0.6$  meV were extracted from DFT calculations [9] for RuO<sub>2</sub>. Their distinct values originate from spin-splitting of electronic band structure of altermagnet.

The spectrum of noninteracting magnon in antiferromagnets is derived [44] standardly from HP-transformed [10] effective spin Hamiltonian [Eq. (3)] in terms of bosonic operators

$$\hat{S}_{i,A}^z = \frac{1}{2} - \hat{a}_i^\dagger \hat{a}_i, \quad \hat{S}_{i,B}^z = \hat{b}_i^\dagger \hat{b}_i - \frac{1}{2}, \quad (4a)$$

$$\hat{S}_{i,A}^- = \sqrt{1 - \hat{a}_i^\dagger \hat{a}_i} \hat{a}_i, \quad \hat{S}_{i,B}^- = \hat{b}_i^\dagger \sqrt{1 - \hat{b}_i^\dagger \hat{b}_i}, \quad (4b)$$

$$\hat{S}_{i,A}^+ = \hat{a}_i^\dagger \sqrt{1 - \hat{a}_i^\dagger \hat{a}_i}, \quad \hat{S}_{i,B}^+ = \sqrt{1 - \hat{b}_i^\dagger \hat{b}_i} \hat{b}_i, \quad (4c)$$

after such transformations are *linearized*— $\hat{S}_{i,A(B)}^z = \frac{1}{2} - \hat{a}_i^\dagger \hat{a}_i (-\frac{1}{2} + \hat{b}_i^\dagger \hat{b}_i)$ ,  $\hat{S}_{i,A(B)}^- = \hat{a}_i (\hat{b}_i^\dagger)$ , and  $\hat{S}_{i,A(B)}^+ = \hat{a}_i^\dagger (\hat{b}_i)$ —and the resulting truncated HP Hamiltonian retains only the lowest order terms [7, 44, 45]. In other words, one performs expansion in  $1/S$ , starting with the order  $1/S^2$ , and retains only terms up to the order  $(1/S)^{-1} = S$  [44]. Here  $A$  and  $B$  denote two sublattices of an antiferromagnet;  $\hat{a}_i (\hat{a}_i^\dagger)$  and  $\hat{b}_i (\hat{b}_i^\dagger)$  destroy (create) a boson at site  $i$  within sublattice  $A$  or  $B$ , respectively; and Eq. (4a) clarifies that number of such bosonic excitations at site  $i$ , as described by operators  $\hat{a}_i^\dagger \hat{a}_i$  and  $\hat{b}_i^\dagger \hat{b}_i$ , captures deviation of magnetic quantum number from its maximum value  $S = 1/2$ . The same strategy leading to truncated [7] HP Hamiltonian that is quadratic in bosonic operators and, therefore, exactly diagonalizable can be applied to altermagnets. For this purpose, one also applies the Bogoliubov-Valatin transformation [44] of  $\hat{a}_i (\hat{a}_i^\dagger)$  and  $\hat{b}_i (\hat{b}_i^\dagger)$  into  $\hat{\alpha}_i (\hat{\alpha}_i^\dagger)$  and  $\hat{\beta}_i (\hat{\beta}_i^\dagger)$ . For Hamiltonian in Eq. (3), this procedure yields HP Hamiltonian of altermagnet RuO<sub>2</sub> truncated to quadratic terms as

$$\hat{H}_{\text{HP}}^{(2)} = -NS^2 \left( J - \frac{J_A}{2} - \frac{J_B}{2} \right) + \sum_{\mathbf{q}} \hbar\omega_A(\mathbf{q}) (\hat{\alpha}_{\mathbf{q}}^\dagger \hat{\alpha}_{\mathbf{q}} + 1/2) + \hbar\omega_B(\mathbf{q}) (\hat{\beta}_{\mathbf{q}}^\dagger \hat{\beta}_{\mathbf{q}} + 1/2). \quad (5)$$

Here we make explicit the zero-point energy terms,  $\hbar\omega(\mathbf{q})/2$ , as second-quantized description of entangled ground state (GS) of quantum altermagnet or antiferromagnet [48–50]. We also keep the (first) constant term which, together with zero-point energy terms, gives for the GS energy of altermagnet

$$E_{\text{GS}} = -NS^2 \left( J - \frac{J_A}{2} - \frac{J_B}{2} \right) - \sum_{\mathbf{q}} \frac{\hbar}{2} \sqrt{\omega_{AB}^2(\mathbf{q}) - 4\gamma(\mathbf{q})}, \quad (6)$$

where  $\gamma(\mathbf{q})$  is standardly used function [44] that encodes the crystalline lattice and its spatial dimensionality. Note that although HP bosonization scheme describes excitations away from the Néel GS, which is not the true (i.e., the lowest energy) GS of collinear quantum antiferromagnets [48, 49], it actually produces GS energy [Eq. (6)] that is close to numerical or analytical (such as Bethe ansatz in 1D) exact values. From Eq. (5) we also read the energy-momentum dispersion of two *non-degenerate* magnon bands

$$\hbar\omega(\mathbf{q}) = \pm \frac{\hbar}{2} [\omega_A(\mathbf{q}) - \omega_B(\mathbf{q})] + \frac{\hbar}{2} \sqrt{\omega_{AB}^2(\mathbf{q}) - 4\gamma(\mathbf{q})}, \quad (7)$$

which are plotted as red sharp lines in Fig. 1 for the case of ladder of square lattice sites whose  $\gamma(q_x) = J \cos q_x a$ . For such quasi-1D lattice, where  $\mathbf{q} \mapsto q_x$ , we also use  $\omega_{AB}(q_x) = \omega_A(q_x) + \omega_B(q_x)$ ;  $\omega_A(q_x) = J - J_A(1 - \cos 2q_x a)$ ;  $\omega_B(q_x) = J - J_B(1 - \cos 2q_x a)$ ; and  $a$  is the lattice constant.

To take into account all possible magnon-magnon interactions—as described by an infinite series [7, 45] (or finite, when such infinite series is properly resummed [7, 51, 52]) of higher order terms on the top of lowest-order HP Hamiltonian in Eq. (5)—we employ TDVP [29, 34, 53] as implemented in ITensor package [54]. Using TDVP, on a ladder of two sites in the transverse direction and  $N = 300$  sites in the longitudinal direction, we follow the same scheme of Ref. [30] to obtain the numerically exact magnon GF

$$G(x, t) = -i\hbar \langle \Psi_0 | \hat{S}_x^-(t) \hat{S}_x^+(0) | \Psi_0 \rangle, \quad (8)$$

and the corresponding spectral function [Eq. (2)]. Note that demonstration of how to obtain these two quantities was originally done via tDMRG algorithm applied to quantum spin chains [30]. The GS  $|\psi_0\rangle$  is found using up to 30 sweeps and a maximum bond dimension  $\chi = 200$ , which guarantees a maximum error of  $\mathcal{O}(10^{-10})$ . Then a wavepacket is created by applying  $\hat{S}_c^+ |\psi_0\rangle$  [30], where  $c = 150$  is the lattice site in the middle of the ladder. Time evolution dynamics was computed using the TDVP algorithm with the same maximum bond dimension, a time step  $\delta t = 0.1(\hbar/J)$ , and a total propagation time of  $22(\hbar/J)$  [which guarantees a maximum error of  $\mathcal{O}(10^{-6})$ ]. The magnon spectral function in Eq. (2) is then obtained as the Fourier transform of Eq. (8) to frequency and momentum, where a Gaussian windowing function for the

Fourier transform in time is typically employed [30]. Note that such windowing function can introduce an artificial broadening of magnon dispersion [30], such as broadening seen outside of the boundaries delineated by the red lines in Fig. 1, but the principal reason for broadened dispersions in Fig. 1 remains magnon-magnon interactions.

Classical ASD simulations were performed using UpASD package [27] in order to compute the dynamical structure factor [26]

$$S^\alpha(\mathbf{q}, \omega) = \frac{1}{\sqrt{2\pi N}} \sum_{\mathbf{r}, \mathbf{r}'} e^{i\mathbf{q} \cdot (\mathbf{r} - \mathbf{r}')} \int_{-\infty}^{\infty} dt e^{i\omega t} C^\alpha(\mathbf{r} - \mathbf{r}', t). \quad (9)$$

Here  $\alpha = x, y, z$ ;  $N$  is the number of atoms per cell; and  $C^\alpha(\mathbf{r} - \mathbf{r}', t) = \overline{M_{\mathbf{r}}^\alpha(t) M_{\mathbf{r}'}^\alpha(0)} - \overline{M_{\mathbf{r}}^\alpha(t)} \overline{M_{\mathbf{r}'}^\alpha(0)}$  measures correlations between spins. The spins in ASD are viewed as classical vectors of fixed length [27, 28] subjected to LLG dynamics and localized at different sites  $\mathbf{r}$  and  $\mathbf{r}'$ , where  $\overline{\dots}$  denotes ensemble average. The ensemble averaging is performed over different time segments during which a system of coupled stochastic (to include temperature [28]) LLG equations is solved to obtain trajectories  $\mathbf{M}_{\mathbf{r}}(t)$ . The dynamical structure factor is directly measurable in neutron scattering experiments on bulk materials, or it can be obtained from spin-polarized high resolution electron energy loss spectroscopy measurements on thin films [26]. By plotting  $S^\alpha(\mathbf{q}, \omega)$  in reciprocal space and by identifying the energies where its peaks appear [26], we extract the energy-momentum dispersion of magnons [Fig. 2], in complete analogy to how dispersion is extracted from experimental neutron scattering data.

*Results and discussion.*—The discrepancy between *noninteracting* (as obtained from HP Hamiltonian in Eq. (5) that is truncated to quadratic terms in boson operators [37]) and *interacting* [16, 37] (as obtained from TDVP) magnon dispersions in Fig. 1(c) is *significant* for the same effective spin Hamiltonian [Eq. (3)] of RuO<sub>2</sub> altermagnet employed in Ref. [9]. That is, sharp HP bands track broadened interacting magnon bands *only* at the Brillouin zone (BZ) center or edges, while deviating substantially in other regions of BZ where broadening due to magnon-magnon interactions concurrently increases. By comparing Figs. 1(c) and 1(a), where the latter employs closer values of two exchange interaction constants  $J_A$  and  $J_B$  between NN spins within sublattices  $A$  and  $B$  respectively, we fully explain this discrepancy as originating from frustration. Such possibility of failure of linearized HP theory of noninteracting magnon dispersion was already emphasized in prior studies on antiferromagnets [16, 36, 37].

The success of coupled LLG equations in modeling numerically, via micromagnetics [55] or ASD [28] codes, classical magnetization dynamics within ferromagnets has also motivated their application to modeling either macrospin magnetization of two sublattices of antiferro-



magnets [46] or individual localized spins on each site of those two sublattices [47]. However, it is well-known that GS of antiferromagnets is entangled [48, 49], as signified by the zero-point energy term we obtain in Eq. (6) for altermagnet as well. Entanglement in the GS of quasi-1D antiferromagnets was also witnessed very recently via neutron scattering experiments [56]. Furthermore, when antiferromagnets are pushed out of equilibrium, additional entanglement is produced due to sampling of excited states, which is not necessarily diminished (especially for spin  $S = 1/2$  and  $S = 1$ ) by the interaction with a dissipative environment [50]. Thus, any nonzero entanglement makes classical description via LLG equation *inapplicable*. Nevertheless, ASD calculations do give us a straightforward access to magnon spectrum at finite temperature and in the presence of magnon-magnon interactions. It is also interesting to compare how well ASD calculations can mimic quantum many-body calculations, taking into account widespread usage [26–28, 55] of LLG-based methods in magnetism. Surprisingly, classical ASD-computed (at  $T = 10$  K) lower magnon band in Fig. 2(c) mimics closely the same band computed by TDVP (at  $T = 0$  K) in Fig. 1(c). That is, because of magnon-magnon interactions captured by nonlinearity of the LLG equation, ASD-computed lower magnon band [Fig. 2(c)] is far more accurate than linearized HP theory-computed lower magnon band [lower red line in Fig. 1(c)]. Nevertheless, magnon-magnon interactions captured quantum-mechanically and nonperturbatively by TDVP calculations are broadening lower magnon band much more than obtained from ASD calculations. The upper bands in Fig. 1(c) and Fig. 2(c) are substantially mismatched. As expected [26], ASD calculations at  $T = 300$  K produce broader version [Figs. 2(b) and 2(d)] of magnon bands [Figs. 2(a) and 2(c)] obtained at  $T = 10$  K. Overall, comparison of Figs. 1 and 2 demonstrates that LLG equation-based methods [26, 46, 47] are not reliable route for computing antiferromagnetic or altermagnetic magnon spectrum.

*Experimental testing of our predictions via Raman scattering.*—Raman scattering (RS), based on inelastic scattering of light [57–61] where the kinetic energy of an incident photon is increased (Stokes RS) or reduced (anti-Stokes RS) during interaction, offers a unique probe of collective excitations in solids, such as magnons (as quanta of spin waves) or phonons (as quanta of lattice vibrations). In experiments, one has to differentiate their signal [61], as it can be done by using the fact that the most striking difference between the phonon and magnon Raman spectra is the temperature dependence of the latter, as well as that the Raman tensor for one-magnon scattering is antisymmetric [59]. Although RS probing of magnons lacks momentum dependence of neutron scattering experiments [15], it provides *high energy* resolution. Such feature of RS makes it possible to correlate sharp peaks in density of states (DOS) of one [59] or two-

magnon excitations [59, 60] to sharp peaks in the Raman spectra. For example, in the case of one-magnon dispersion in Fig. 1(c), we find the *flat-topped portion* of the dispersion around the BZ center leads to sharp peaks in the DOS, which should be accessible to RS experimental detection.

*Conclusions.*—By comparing dispersions of *interacting vs. noninteracting* magnons in altermagnet  $\text{RuO}_2$ —as computed, respectively, from numerically (quasi)exact quantum many-body calculations via TDVP (in quasi-1D ladder geometry required by this methodology [34, 35]) vs. recently reported [9] quantum one-body calculations via linearized HP transformations—we unravel their *significant discrepancy* [Fig. 1(c)]. The discrepancy signals the importance of magnon-magnon interactions [16, 37] leading to spontaneous magnon decay [16] and thereby generated *broadening and shifting* [Fig. 1(c)] of noninteracting magnon bands. It is traced back [Fig. 1(c) vs. Fig. 1(a)] to large difference [9] in exchange interactions within two sublattices of altermagnet (an atlas of other cases where linearized HP calculations can fail can be found in Refs. [16, 37]). We also divulge how popular ASD simulations [26–28, 55] based on the stochastic LLG equation, which can take into account magnon-magnon interactions and finite temperature but *not* any quantum effects, are generally unwarranted for the cases of antiferromagnetic (despite widespread usage [12, 46]) and altermagnetic magnon dispersions (Fig. 1 vs. 2). This can be traced back to highly nonclassical effects [48, 49, 56] which antiferromagnetic materials can harbor, persisting even at higher temperatures [56] and especially out of equilibrium [50]. Nevertheless, LLG equation-based simulations to obtain ferromagnetic [26, 27] magnon spectra can be rigorously justified [50].

This research was supported by the US National Science Foundation (NSF) through the University of Delaware Materials Research Science and Engineering Center, DMR-2011824. The supercomputing time was provided by DARWIN (Delaware Advanced Research Workforce and Innovation Network), which is supported by NSF Grant No. MRI-1919839. The paper originated from Research Projects Based Learning implemented within a graduate course *PHYS800: Advanced Graduate Seminar in Quantum Physics* [62] at the University of Delaware.

---

\* [bnikolic@udel.edu](mailto:bnikolic@udel.edu)

- [1] E. Kaxiras and J. D. Joannopoulos, *Quantum theory of materials* (Cambridge University Press, Cambridge, 2019).
- [2] S. Konschuh, M. Gmitra, and J. Fabian, Tight-binding theory of the spin-orbit coupling in graphene, *Phys. Rev. B* **82**, 245412 (2010).
- [3] E. Kogan, V. U. Nazarov, V. M. Silkin, and M. Kaveh,

- Energy bands in graphene: Comparison between the tight-binding model and ab initio calculations, *Phys. Rev. B* **89**, 165430 (2014).
- [4] K. Held, Electronic structure calculations using dynamical mean field theory, *Adv. Phys.* **56**, 829 (2007).
- [5] M. D. Watson, S. Backes, A. A. Haghighirad, M. Hoesch, T. K. Kim, A. I. Coldea, and R. Valentí, Formation of Hubbard-like bands as a fingerprint of strong electron-electron interactions in FeSe, *Phys. Rev. B* **95**, 081106 (2017).
- [6] F. Bloch, Zur theorie des ferromagnetismus, *Z. Phys.* **61**, 206 (1930).
- [7] U. Bajpai, A. Suresh, and B. K. Nikolić, Quantum many-body states and Green's functions of nonequilibrium electron-magnon systems: Localized spin operators versus their mapping to Holstein-Primakoff bosons, *Phys. Rev. B* **104**, 184425 (2021).
- [8] A. Szilva, Y. Kvashnin, E. A. Stepanov, L. Nordström, O. Eriksson, A. I. Lichtenstein, and M. I. Katsnelson, Quantitative theory of magnetic interactions in solids, *Rev. Mod. Phys.* **95**, 035004 (2023).
- [9] L. Šmejkal, A. Marmodoro, K.-H. Ahn, R. González-Hernández, I. Turek, S. Mankovsky, H. Ebert, S. W. D'Souza, O. Šipr, J. Sinova, and T. Jungwirth, Chiral magnons in altermagnetic RuO<sub>2</sub>, *Phys. Rev. Lett.* **131**, 256703 (2023).
- [10] T. Holstein and H. Primakoff, Field dependence of the intrinsic domain magnetization of a ferromagnet, *Phys. Rev.* **58**, 1098 (1940).
- [11] T. Olsen, Unified treatment of magnons and excitons in monolayer CrI<sub>3</sub> from many-body perturbation theory, *Phys. Rev. Lett.* **127**, 166402 (2021).
- [12] Y. Li and W. Bailey, Wave-number-dependent Gilbert damping in metallic ferromagnets, *Phys. Rev. Lett.* **116**, 117602 (2016).
- [13] L. Chen, C. Mao, J.-H. Chung, M. B. Stone, A. I. Kolesnikov, X. Wang, N. Murai, B. Gao, O. Delaire, and P. Dai, Anisotropic magnon damping by zero-temperature quantum fluctuations in ferromagnetic CrGeTe<sub>3</sub>, *Nat. Commun.* **13**, 4037 (2022).
- [14] P. Dai, H. Y. Hwang, J. Zhang, J. A. Fernandez-Baca, S.-W. Cheong, C. Kloc, Y. Tomioka, and Y. Tokura, Magnon damping by magnon-phonon coupling in manganese perovskites, *Phys. Rev. B* **61**, 9553 (2000).
- [15] S. P. Bayraktci, D. A. Tennant, P. Leininger, T. Keller, M. C. R. Gibson, S. D. Wilson, R. J. Birgeneau, and B. Keimer, Lifetimes of antiferromagnetic magnons in two and three dimensions: Experiment, theory, and numerics, *Phys. Rev. Lett.* **111**, 017204 (2013).
- [16] M. E. Zhitomirsky and A. L. Chernyshev, *Colloquium*: Spontaneous magnon decays, *Rev. Mod. Phys.* **85**, 219 (2013).
- [17] A. Chumak, V. Vasyuchka, A. Serga, and B. Hillebrands, Magnon spintronics, *Nat. Phys.* **11**, 453 (2015).
- [18] A. V. Chumak, P. Kabos, M. Wu, C. Abert, C. Adelmann, A. O. Adeyeye, J. Akerman, F. G. Aliev, A. Anane, A. Awad, *et al.*, Advances in magnetics roadmap on spin-wave computing, *IEEE Trans. Magn.* **58**, 1 (2022).
- [19] P. Buczek, A. Ernst, P. Bruno, and L. M. Sandratskii, Energies and lifetimes of magnons in complex ferromagnets: A first-principle study of Heusler alloys, *Phys. Rev. Lett.* **102**, 247206 (2009).
- [20] N. Tancogne-Dejean, F. Eich, and A. Rubio, Time-dependent magnons from first principles, *J. Chem. Theory Comput.* **16**, 1007 (2020).
- [21] E. Hankiewicz, G. Vignale, and Y. Tserkovnyak, Inhomogeneous Gilbert damping from impurities and electron-electron interactions, *Phys. Rev. B* **78**, 020404(R) (2008).
- [22] Y. Tserkovnyak, E. M. Hankiewicz, and G. Vignale, Transverse spin diffusion in ferromagnets, *Phys. Rev. B* **79**, 094415 (2009).
- [23] F. Reyes-Osorio and B. K. Nikolić, Nonlocal damping of spin waves in a magnetic insulator induced by normal, heavy, or altermagnetic metallic overlayer: A Schwinger-Keldysh field theory approach, arXiv:2312.09140 (2023).
- [24] P. M. Bonetti and W. Metzner, Spin stiffness, spectral weight, and Landau damping of magnons in metallic spiral magnets, *Phys. Rev. B* **105**, 134426 (2022).
- [25] R. L. Smit, S. Keupert, O. Tsypliyatyev, P. A. Maksimov, A. L. Chernyshev, and P. Kopietz, Magnon damping in the zigzag phase of the Kitaev-Heisenberg-Γ model on a honeycomb lattice, *Phys. Rev. B* **101**, 054424 (2020).
- [26] C. Etz, L. Bergqvist, A. Bergman, A. Taroni, and O. Eriksson, Atomistic spin dynamics and surface magnons, *J. Condens. Matter Phys.* **27**, 243202 (2015).
- [27] B. Skubic, J. Hellsvik, L. Nordström, and O. Eriksson, A method for atomistic spin dynamics simulations: implementation and examples, *J. Condens. Matter Phys.* **20**, 315203 (2008).
- [28] R. Evans, W. Fan, P. Chureemart, T. Ostler, M. O. Ellis, and R. Chantrell, Atomistic spin model simulations of magnetic nanomaterials, *J. Phys.: Condens. Matter* **26**, 103202 (2014).
- [29] S. Paeckel, T. Köhler, A. Swoboda, S. Manmana, U. Schollwöck, and C. Hubig, Time-evolution methods for matrix-product states, *Ann. Phys.* **411**, 167998 (2019).
- [30] S. R. White and A. E. Feiguin, Real-time evolution using the density matrix renormalization group, *Phys. Rev. Lett.* **93**, 076401 (2004).
- [31] A. Daley, C. Kollath, U. Schollwöck, and G. Vidal, Time-dependent density-matrix renormalization-group using adaptive effective hilbert spaces, *JSTAT* **2004** (04), P04005.
- [32] P. Schmitteckert, Nonequilibrium electron transport using the density matrix renormalization group method, *Phys. Rev. B* **70**, 121302 (2004).
- [33] A. E. Feiguin, The density matrix renormalization group and its time-dependent variants, *AIP Conf. Proc.* **1419**, 5 (2011).
- [34] J. Haegeman, C. Lubich, I. Oseledets, B. Vandereycken, and F. Verstraete, Unifying time evolution and optimization with matrix product states, *Phys. Rev. B* **94**, 165116 (2016).
- [35] T. Chanda, P. Sierant, and J. Zakrzewski, Time dynamics with matrix product states: Many-body localization transition of large systems revisited, *Phys. Rev. B* **101**, 035148 (2020).
- [36] M. Mourigal, W. T. Fuhrman, A. L. Chernyshev, and M. E. Zhitomirsky, Dynamical structure factor of the triangular-lattice antiferromagnet, *Phys. Rev. B* **88**, 094407 (2013).
- [37] M. Gohlke, A. Corticelli, R. Moessner, P. A. McClarty, and A. Mook, Spurious symmetry enhancement in linear spin wave theory and interaction-induced topology in magnons, *Phys. Rev. Lett.* **131**, 186702 (2023).
- [38] L. Šmejkal, J. Sinova, and T. Jungwirth, Emerging re-

- search landscape of altermagnetism, *Phys. Rev. X* **12**, 040501 (2022).
- [39] L. Šmejkal, J. Sinova, and T. Jungwirth, Beyond conventional ferromagnetism and antiferromagnetism: A phase with nonrelativistic spin and crystal rotation symmetry, *Phys. Rev. X* **12**, 031042 (2022).
- [40] S. Hayami, Y. Yanagi, and H. Kusunose, Momentum-dependent spin splitting by collinear antiferromagnetic ordering, *J. Phys. Soc. Jpn.* **88**, 23702 (2019).
- [41] L.-D. Yuan, Z. Wang, J.-W. Luo, E. I. Rashba, and A. Zunger, Giant momentum-dependent spin splitting in centrosymmetric low- $z$  antiferromagnets, *Phys. Rev. B* **102**, 014422 (2020).
- [42] L. Šmejkal, R. González-Hernández, T. Jungwirth, and J. Sinova, Crystal time-reversal symmetry breaking and spontaneous hall effect in collinear antiferromagnets, *Sci. Adv.* **6**, eaaz8809 (2020).
- [43] I. I. Mazin, K. Koepf, M. D. Johannes, R. González-Hernández, and L. Šmejkal, Prediction of unconventional magnetism in doped FeSb<sub>2</sub>, *PNAS* **118**, e2108924118 (2021).
- [44] E. M. Chudnovsky and J. Tejada, *Lectures on Magnetism* (Rinton Press, Princeton, 2006).
- [45] S. Zheng, Z. Wang, Y. Wang, F. Sun, Q. He, P. Yan, and H. Yuan, Tutorial: Nonlinear magnonics, *J. Appl. Phys.* **134**, 151101 (2023).
- [46] R. Cheng, J. Xiao, Q. Niu, and A. Brataas, Spin pumping and spin-transfer torques in antiferromagnets, *Phys. Rev. Lett.* **113**, 057601 (2014).
- [47] P. Li, J. Chen, R. Du, and X.-P. Wang, Numerical methods for antiferromagnets, *IEEE Trans. Magn.* **56**, 1 (2020).
- [48] H. F. Song, N. Laflorencie, S. Rachel, and K. Le Hur, Entanglement entropy of the two-dimensional Heisenberg antiferromagnet, *Phys. Rev. B* **83**, 224410 (2011).
- [49] A. Kamra, W. Belzig, and A. Brataas, Magnon-squeezing as a niche of quantum magnonics, *Appl. Phys. Lett.* **117**, 090501 (2020).
- [50] F. Garcia-Gaitan and B. K. Nikolić, The fate of entanglement in ferro- and antiferro-magnets under Lindbladian or non-markovian dynamics and possible transition to Landau-Lifshitz classical dynamics, arXiv:2303.17596 (2023).
- [51] M. Vogl, P. Laurell, H. Zhang, S. Okamoto, and G. A. Fiete, Resummation of the Holstein-Primakoff expansion and differential equation approach to operator square roots, *Phys. Rev. Res.* **2**, 043243 (2020).
- [52] J. König and A. Hucht, Newton series expansion of bosonic operator functions, *SciPost Phys.* **10**, 007 (2021).
- [53] M. Yang and S. R. White, Time-dependent variational principle with ancillary Krylov subspace, *Phys. Rev. B* **102**, 094315 (2020).
- [54] M. Fishman, S. R. White, and E. M. Stoudenmire, The ITensor software library for tensor network calculations, *SciPost Phys. Codebases*, 4 (2022).
- [55] D. V. Berkov and J. Miltat, Spin-torque driven magnetization dynamics: Micromagnetic modeling, *J. Magn. Mater.* **320**, 1238 (2008).
- [56] A. Scheie, P. Laurell, A. M. Samarakoon, B. Lake, S. E. Nagler, G. E. Granroth, S. Okamoto, G. Alvarez, and D. A. Tennant, Witnessing entanglement in quantum magnets using neutron scattering, *Phys. Rev. B* **103**, 224434 (2021).
- [57] T. P. Devereaux and R. Hackl, Inelastic light scattering from correlated electrons, *Rev. Mod. Phys.* **79**, 175 (2007).
- [58] P. Lemmens, G. Güntherodt, and C. Gros, Magnetic light scattering in low-dimensional quantum spin systems, *Phys. Rep.* **375**, 1 (2003).
- [59] P. A. Fleury and R. Loudon, Scattering of light by one- and two-magnon excitations, *Phys. Rev.* **166**, 514 (1968).
- [60] M. Cottam, Theory of two-magnon Raman scattering in antiferromagnets at finite temperatures, *J. Phys. C: Solid State Phys.* **5**, 1461 (1972).
- [61] M. T. Hutchings, M. F. Thorpe, R. J. Birgeneau, P. A. Fleury, and H. J. Guggenheim, Neutron and optical investigation of magnons and magnon-magnon interaction effects in NiF<sub>2</sub>, *Phys. Rev. B* **2**, 1362 (1970).
- [62] <https://wiki.physics.udel.edu/phys800>.